Applied Physics B, February 2013, Volume 110, Issue 2, pp 223-231

Using integrating spheres with wavelength modulation spectroscopy: effect of pathlength distribution on 2nd harmonic signals

J Hodgkinson[*]*, D Masiyano[*,†] and R P Tatam[*]*

corresponding author j.hodgkinson@cranfield.ac.uk

* Department of Engineering Photonics, School of Engineering, Cranfield University, Bedfordshire, MK43 0AL, UK.

† Now at: Two Trees Photonics* (UK) Ltd, 23 Roebuck Way, Beaufort Court, Knowhill, Milton Keynes, MK5 8HL, UK.

Abstract

We have studied the effect on 2nd harmonic wavelength modulation spectroscopy of the use of integrating spheres as multipass gas cells. The gas lineshape becomes distorted at high concentrations, as a consequence of the exponential pathlength distribution of the sphere, introducing nonlinearity beyond that expected from the Beer-Lambert law. We have modelled this numerically for methane absorption at 1.651 μm, with gas concentrations in the range of 0-2.5%vol in air. The results of this model compare well with experimental measurements. The nonlinearity for the 2*f* WMS measurements is larger than that for direct scan measurements; if this additional effect were not accounted for, the resulting error would be approximately 20% of the reading at a concentration of 2.5 %vol methane.

PACS codes

07.07.Df	sensors – chemical	42.79.-e	optical instruments, equipment and techniques
42.62.Fi	laser spectroscopy		

1 Introduction

The detection and quantification of gas concentrations by measurement of their optical absorption is a technique with great scientific and commercial importance. Many methods have been devised to improve the signal to noise ratio (SNR) of this technique by extending the optical pathlength in gas sample cells. Multipass cells have been designed by White[1], Herriott et al.[2] and Chernin and Barskaya[3]. As the description suggests, the light makes multiple passes across the cell, ideally without any overlap between beams at the detector. Cavity-enhanced techniques employing high quality dielectric mirrors (with reflectivity in excess of 99.999%) include integrated cavity output spectroscopy, ICOS, also termed cavity enhanced absorption spectroscopy[4] and cavity ringdown spectroscopy, CRDS[5]. Pathlengths of over 10 km can be reached within a physical length of 1 m[5]). Here, beams are encouraged to overlap and over

time the detector measures a series of light beams that have made increasing numbers of passes, such that with each pass a small fraction of the light leaves the cell and lands on the detector.

Integrating spheres have great promise as multipass gas cells that require minimal optical alignment in both broadband measurements[6,7] and tunable diode laser spectroscopy[8,9,10]. Light entering the sphere is scattered by the internal walls with very high levels of total diffuse reflectance. This geometry disrupts the formation of etalons within the cell, which in conventional cells would be performance - limiting[11] . However it also creates a random interference phenomenon – laser speckle – that must be minimised in order to realise the SNR benefits of the longer pathlength[12]. For the measurement geometry described in this paper, we have previously estimated the noise equivalent absorbance (NEA) in direct spectral scans to be 5×10^{-5} (short term) and 4×10^{-4} (drift over a 21-hour period)[12].

For an ideal Lambertian surface and a cavity with spherical geometry, the irradiance received from any point is uniform over the sphere[13]. As shown in Figure 1, collimated light entering the sphere hits the "first strike spot" and from then on is randomly scattered, making multiple passes across the sphere. With each pass, a small fraction of the light is lost at the inner surface of the sphere, the detector, and any apertures such as the entrance window and gas inlet / outlet. Because of the spherical geometry, the detector measures a representative fraction of the inner irradiance. The fact that multiple light beams overlap means that their optical pathlength distribution is similar to that in cavity-enhanced techniques, and indeed measurement of the impulse response of integrating spheres shows an exponential decay[14], as in CRDS.

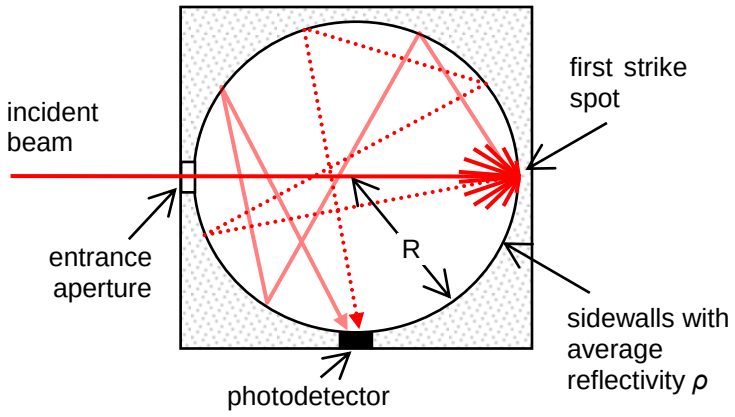

Figure 1. Simplified model of an integrating sphere, showing a collimated beam making a first pass across the cell to the first strike spot. Two examples are shown of light beams making subsequent random multiple passes across the cell.

We have previously modelled the optical pathlength distribution in an integrating sphere used as a multipass optical cell for TDLS and its effect on the transfer function of the integrating sphere[15]. At high concentrations, in the nonlinear region of the Beer-Lambert law (Eq. (1) below), the effect is a predictable nonlinearity of the measurement, which we have validated experimentally using direct spectral scans. The

nonlinearity goes beyond what would normally be expected of a cell with a single pathlength, and its form is a consequence of an exponential distribution of optical pathlengths. In this paper, we have extended our analysis to cover the effect on measurements made using second harmonic wavelength modulation spectroscopy (2*f* WMS) resulting from nonlinear distortion of the gas lineshape. 2*f* WMS is commonly used in TDLS but is known to be highly sensitive to lineshape changes caused for example by changes in sample pressure. For example, Kan et al. have analysed the effect on 2*f* WMS signals of lineshape distortions in the nonlinear regime of the Beer-Lambert law, Eq. (1) below[16]. However, to our knowledge the effect of distortion induced by the nonlinear transfer function of integrating spheres, or related effects in cavity-enhanced spectroscopy, has not been reported.

2 Theory

2.1 Gas detection

For monochromatic radiation, the radiant flux (in W) transmitted through a gas cell, Φ, is given by the Beer-Lambert law[17]:

$$\Phi(\nu) = \Phi_0 \exp(-\alpha(\nu) z) \tag{1}$$

where Φ_0 is the radiant flux transmitted in the absence of light absorption, z is the pathlength (in cm) and α is the absorption coefficient of the sample, equal to the concentration C of the analyte (in units of partial pressure, atm, equivalent to %vol at atmospheric pressure), multiplied by the specific absorptivity of the gas, ε (in $atm^{-1}\ cm^{-1}$). Both Φ and α are functions of the wavenumber ν in cm^{-1}. At low values of αz, Eq. (1) approximates to the following linear relationship:

$$\frac{\Delta\Phi}{\Phi_0} \approx \alpha z \tag{2}$$

where ΔΦ is the measured change in transmitted radiant flux, Φ_0-Φ, resulting from light absorption.

At atmospheric pressure, a single gas line has a pressure-broadened Lorentzian profile[18], such that

$$\alpha(\nu) = C_{mol} S \frac{\gamma}{\pi\left(\gamma^2 + (\nu - \nu_0)^2\right)} \tag{3}$$

where C_{mol} is the number density of gas molecules in units of molecules cm^{-3}, S is the linestrength (cm^{-1}/molecule cm^{-2}), γ is the line half-width at half-maximum (HWHM, cm^{-1}), ν is the wavenumber (cm^{-1}) and ν_0 is the wavenumber of the line centre. The linewidth γ can change for a gas in different matrices; for a gas in air at a partial pressure P_s and overall pressure P, the value is given by[18]

$$\gamma = \gamma_{air}(P - P_s) + \gamma_{self} P_s \tag{4}$$

where γ_{air} and γ_{self} are the air-broadened and self-broadened parameters, ie the linewidths for gas molecules surrounded by air and by gas matrices, respectively.

2.2 Second harmonic wavelength modulation spectroscopy

In WMS, the laser wavelength is modulated by applying a sinusoidal dither to the injection current at a frequency *f*, such that the wavenumber *v* varies with time *t* as

$$\nu\ t\ = \nu_0 + x\cos\ 2\pi f t \tag{5}$$

where x is the modulation amplitude. The measured signal as a function of time is then

$$V\ t\ = \Phi\ \nu_0 + x\cos\ 2\pi f t \tag{6}$$

A lock-in amplifier is typically used to recover signals at the 2nd harmonic, giving a signal that is mathematically equivalent to the 2*f* Fourier component of the lineshape function[19]. Typically the X component of the signal is recorded, such that

$$V_2\ = \int_{\tau} V\ t\ \cos\ 2\pi f t + \phi\ \mathrm{d}t \tag{7}$$

where V_2 is the magnitude of the 2nd harmonic X component, the cos function is generated from the reference input to the lock-in amplifier, and ϕ and τ are the lock-in amplifier phase and time constant, respectively. The magnitude of the resulting signals was modelled by Arndt[20]. The modulation index m is defined as

$$m = \frac{x}{\gamma} \tag{8}$$

In the linear regime of Eq. (1), the DC normalised signal level is

$$\frac{V_2}{V_0} = -k\alpha z \tag{9}$$

where V_0 is the DC signal and *k* is a function of the modulation index *m*. Arndt showed that for Lorentzian lineshapes the magnitude of 2*f* signals was maximised for *m*=2.2, resulting in *k* = 0.343.

2.3 Integrating spheres

Figure 1 shows a simplified model of the integrating sphere used in our experiments. Fry *et al.*[14] have derived the irradiance *E* (in W m^{-2}) as a function of time, following an impulse:

$$E\ t\ = E_0 \exp\left(-\frac{t}{\tau}\right) \quad \text{and} \quad \tau = -\frac{\bar{t}}{\ln \rho} \tag{10}$$

where $\bar{t}$ is the mean transit time for photons across the cavity and ρ is the mean inner reflectivity of the

sphere; $\bar{t}$ is equal to $c.z_0$ where $z_0 = \frac{4}{3}R$ is the mean pathlength for a single pass across the sphere. The consequence is an optical pathlength distribution that is exponential in character. We have previously shown that for such a distribution, the general transfer function of the sphere is [15]:

$$\frac{\Phi}{\Phi_0} = \frac{\ln\rho}{\ln\rho - \alpha\, z_0} \tag{11}$$

Our work also showed the need for a further term that adds a small extra pathlength ($z_\ell + z_0/2$) to take account of the optical launch and delaunch geometry of the sphere, as follows:

$$\frac{\Phi}{\Phi_0} = \exp\left(-\alpha\left(z_\ell + \frac{z_0}{2}\right)\right) \quad \frac{\ln\rho}{\ln\rho - \alpha\, z_0} \tag{12}$$

The value of both the pathlength z_ℓ and the reflectivity ρ can be determined empirically.

A more recent theoretical study by Manojlovíc and Marinčíc[21], based on an energy conservation analysis, shows that the original relation to lnρ should be replaced by (1-ρ), to give:

$$\frac{\Phi}{\Phi_0} = \exp\left(-\alpha\left(z_\ell + \frac{z_0}{2}\right)\right) \quad \frac{1-\rho}{1-\rho+\alpha z_0} \tag{13}$$

In practice at high levels of reflectivity, the difference between Eqs. (12) and (13) is negligible (less than 1% difference for ρ > 96%).

Under conditions of zero gas absorption, an equivalent pathlength Z_{eff} can be defined for the cell as follows, using the analysis of Fry et al.[22] plus our additional pathlength.

$$Z_{eff} = \frac{z_0}{1-\rho} + \frac{z_0}{2} + z_\ell \tag{14}$$

Note that Z_{eff} is a sensitive function of the mean surface reflectivity, ρ. This parameter is governed by the reflectivity of the sphere material and by the proportion of non-reflective area taken up by, for example, the entrance aperture, photodetector and housing, plus gas inlet and outlet ports. It is not usually sufficient to calculate ρ by using manufacturer's reflectivity data and knowledge of the cell geometry; instead, cell calibration is required using Eq. (13). Using the procedure outlined in Ref. [15] to calibrate our 5-cm diameter integrating sphere, we obtained values of ρ = 96.4 % and $z_\ell = 2.21\,R$, with an equivalent pathlength of Z_{eff} = 1.02 ± 0.01 m.

3 Numerical modelling

Several authors have provided analytical models to obtain the magnitude of 2*f* WMS signals from a Lorentzian absorption profile[20,23]. However, because of the lineshape distortions introduced by the integrating sphere we were unable to use these models. For the more general case, analytical solutions to the problem do not necessarily exist. Possible alternatives include a numerical replication of lock-in signal

recovery[19], Fourier decomposition of the lineshape, and a convolution model using systems theory to give the WMS profile obtained while scanning across the line[24]. We chose to use the first of these because of its relative ease of numerical processing and its direct link to our experimental method, however all these methods can be considered mathematically equivalent.

Our work concentrates on the R4 quadruplet absorption line of methane at a centre wavelength of $\lambda_0 = 1650.96$ nm, within the $2\nu_3$ absorption band. However, our results are equally applicable to TDLS based gas detection at other wavelengths. Information within the 2008 HITRAN database[25] was used to calculate the composite absorption profile from 4 main underlying transitions and many minor transitions; these are unresolved at atmospheric pressure. We fitted a single Lorentzian profile (according to Eq. (3)) to this line with parameters of $S = (4.02 \pm 0.05) \times 10^{-21}$ cm molecule^{-1} and $\gamma = 0.072 \pm 0.002$ cm^{-1}, the latter corresponding to a wavelength change of $\Delta\lambda = 0.020$ nm or a frequency change of $\Delta\nu = 2.2$ GHz. Figure 2 shows the fitted absorption profile compared with the lineshape calculated from HITRAN parameters. That we were able to produce a good Lorentzian fit confirms that our results can be translated to other absorption lines at atmospheric pressure containing a single transition. The addition of smaller transitions in the "wings" of this line can also be seen, but these lie outside the $\lambda_0 \pm 2.2\ \Delta\lambda$ region.

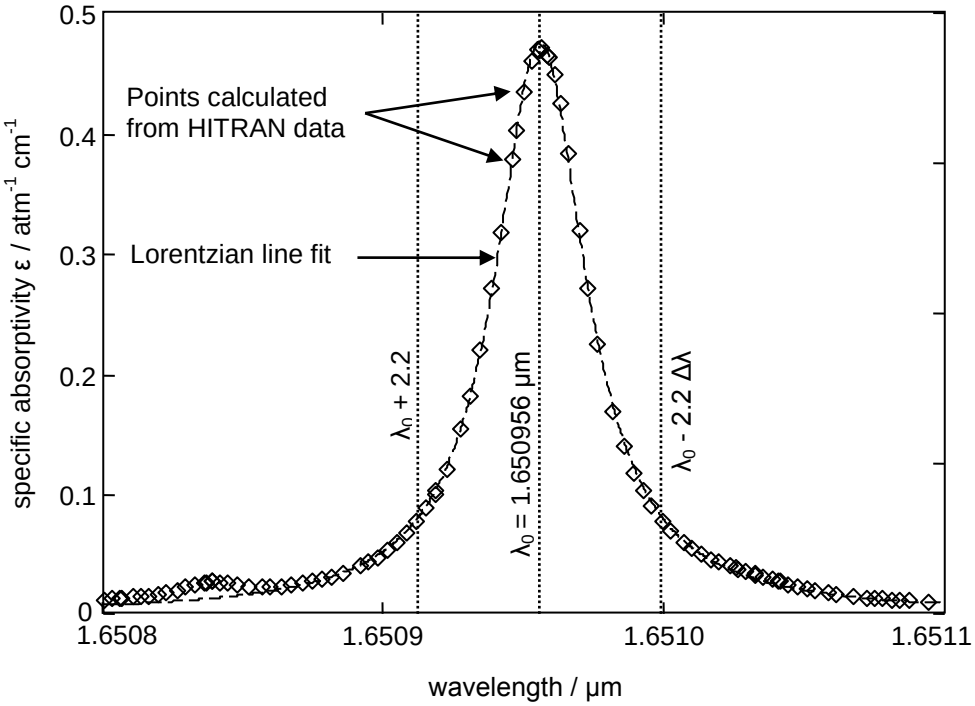

Figure 2. Absorption profile for methane at atmospheric pressure, calculated from data in the HITRAN database, using air-broadened linewidths.

Over the gas concentration range used here (0-2.5 %vol methane in zero air), the absorption linewidth changes slightly because of differences in the air- and self- broadening parameters of Eq. (4). For simplicity we chose to calculate the absorption line profile using the HITRAN air-broadening parameters

for methane as we worked at concentrations up to only 2.5 %vol. Including the self-broadening parameters throughout this model would have increased the model's accuracy but would also have increased the processing time considerably as it involves re-calculating the basic absorption line profile at every concentration step. At a concentration of 2.5 %vol, the resulting error in the linewidth was estimated to be 0.7%, which as we will see is over a factor of 10 smaller than the line broadening due to the cell effects reported here.

The numerical analysis procedure is shown schematically in Figure 3 (all functions being plotted to scale) and consisted of the following steps, completed using the Mathcad^{TM} v14 software package[26].

1. A sinusoidal modulation was constructed according to Eq. (5), with amplitude = 0.044 nm (4.8 GHz), centred on λ_0 = 1.69056 μm, frequency and time arbitrary (but self-consistent within the model). The value of x was determined by the optimal value of m = 2.2 in Eq. (8), as previously discussed. The function was implemented as an array with a total of 500 steps in one cycle. The numerical modulation is plotted to scale as a change in wavelength with time in Figure 3, box (1).
2. A synthetic absorption spectrum for methane was calculated using data in the HITRAN database[18], shown in Figure 2. This spectrum was constructed using 30 data points in the range $\lambda_0 \pm 2\Delta\lambda$, with uneven wavelength spacing (being based on fitted absorption profiles for several underlying spectral transitions). To permit calculation of the modelled signal as a function of time, a lookup function was required that gave a numerical absorption coefficient (α) output for a wavelength input in 500 equally spaced wavelength steps. A simple linear interpolation between the points plotted in Figure 2 provided this lookup function to give the absorptivity ε. A synthetic absorption coefficient $\alpha = \varepsilon C$ was then calculated for the gas concentration, C. To model the integrating sphere, we substituted α into the integrating sphere transfer function, Φ, of Eq. (13). The modelled transmission spectrum is plotted to scale in Figure 3, box (2).
3. At each step change in wavelength during the modulation cycle, the synthetic recovered signal voltage was then calculated according to Eq. (6). The resulting recovered signal is plotted to scale in Figure 3, box (3).
4. Demodulation of the signal in a lock-in amplifier was modelled as follows. First, a sinusoidal reference function was constructed numerically at frequency f, setting the phase to $\phi = 0$ without loss of generality. As in Eq. (7), the synthetic recovered signal of Step 3 was multiplied by this reference, summed over one full cycle and normalised to give the RMS equivalent signal at a frequency $2f$. The intermediate multiplication step and the resulting summed RMS signal are both plotted to scale in Figure 3, box (4).

Steps 1 to 4 were repeated for a range of values of the gas concentration, from 0 to 2.5 %vol.

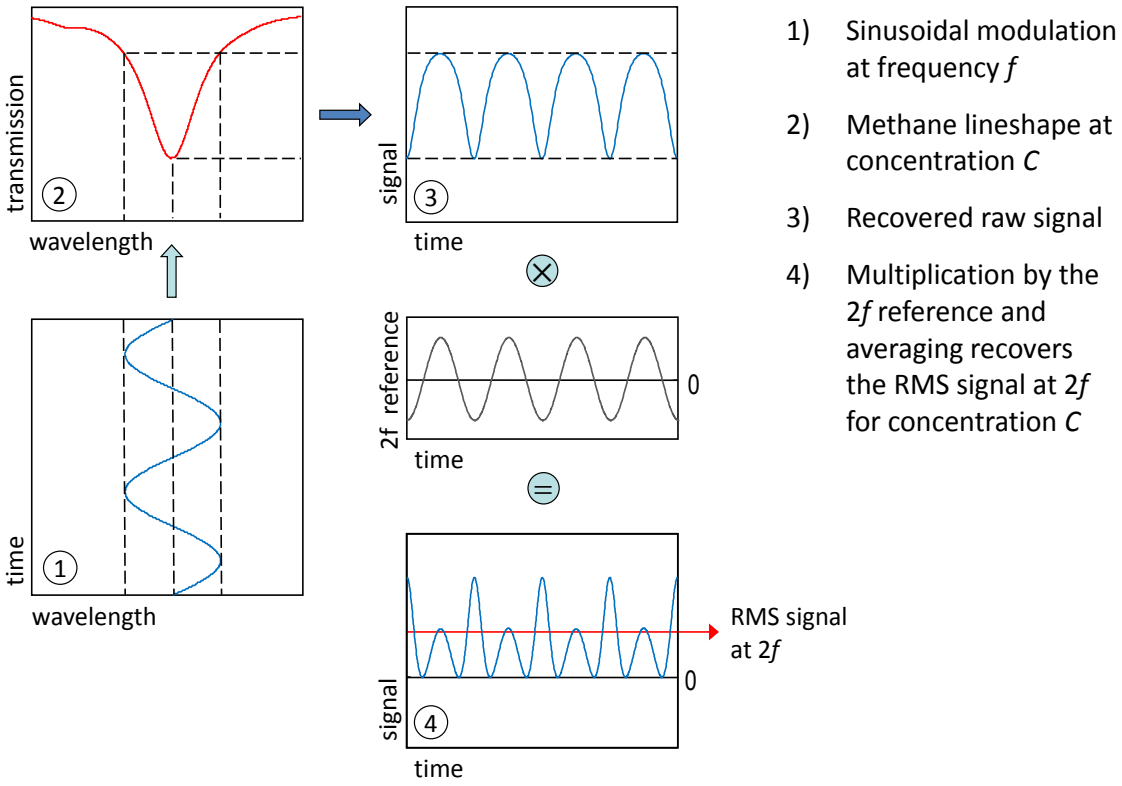

Figure 3. Schematic representation of numerical simulation of 2*f* WMS signal recovery using a lock-in amplifier.

The consequence of the integrating sphere transfer function, Eq. (13), is a distortion of the measured transmission. Figure 4(a) shows the modelled distortion compared to the lineshape normally expected for a single pass cell with the same equivalent pathlength (1.02 m), for the worst case (highest concentration – 2.5 %vol). Note that this distortion goes beyond what is normally expected when working outside the linear regime of the Beer-Lambert law, Eq. (1). For this example, the apparent absorbance is reduced by 19% and the effective linewidth is increased by 12%; the latter effect can more easily be visualised in Figure 4(b), in which the lineshape for the integrating sphere has been rescaled to give it the same peak value. The apparent reduction in absorbance has been previously reported for direct line scans[15]. As WMS is particularly sensitive to changes in linewidth, we expect the linewidth increase to reduce the recovered WMS signals still further.

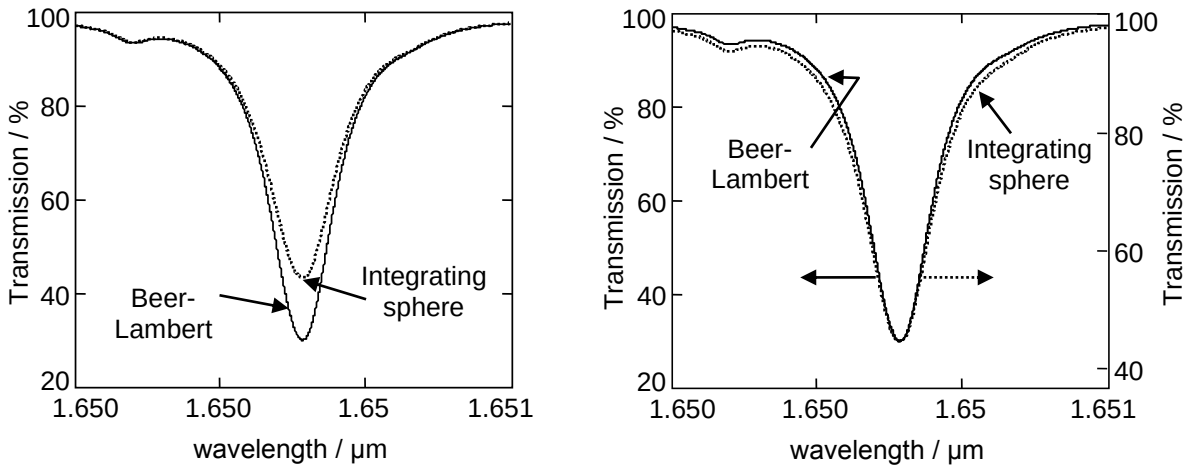

Figure 4. Distortion of measured transmission spectrum for 2.5 %vol methane in air by a 50mm diameter integrating sphere, compared with a single pass cell with the same equivalent pathlength (1.02m). (a) Calculated lineshapes on the same scale, (b) with the integrating sphere lineshape rescaled to show apparent line broadening.

The calculated effect of the line distortion on 2*f* WMS signals is plotted as a function of concentration in Figure 6 below, where the predicted signal levels are compared with experimental measurements.

4 Experimental details

We employed WMS at f = 6 kHz with second harmonic (2*f*) detection at 12 kHz. Figure 5 shows a schematic diagram of our laser diode modulation and detection apparatus. A sinusoidal signal at 6 kHz from a signal generator (Hewlett Packard HP33120A) was applied to the laser controller (ILX Lightwave, ILX LDC-3722B) to give an amplitude at the laser diode of 24mA (peak to peak). Our DFB laser diode package (Semelab Ltd) incorporated a 1651 nm laser (NEL NLK1U5C1CA-TS) collimated with an aspheric lens (Lightpath 350230D). Gross wavelength tuning was achieved by controlling the diode temperature using a Peltier element within the package.

A proportion of the laser beam was sampled by a pellicle beamsplitter (Thorlabs BP245B3, 45:55 split ratio) to a gas reference cell consisting of a Ge detector at the bottom of a TO18 can containing 100% methane, giving an effective pathlength of 5.3mm. The signal from the photodiode was demodulated at 3*f* using a lock-in amplifier (Stanford Research Systems SR850) to provide an error signal which was fed, via a PID (proportional, integral, derivative) controller to the laser current controller, thereby applying a correction to the laser diode DC injection current.

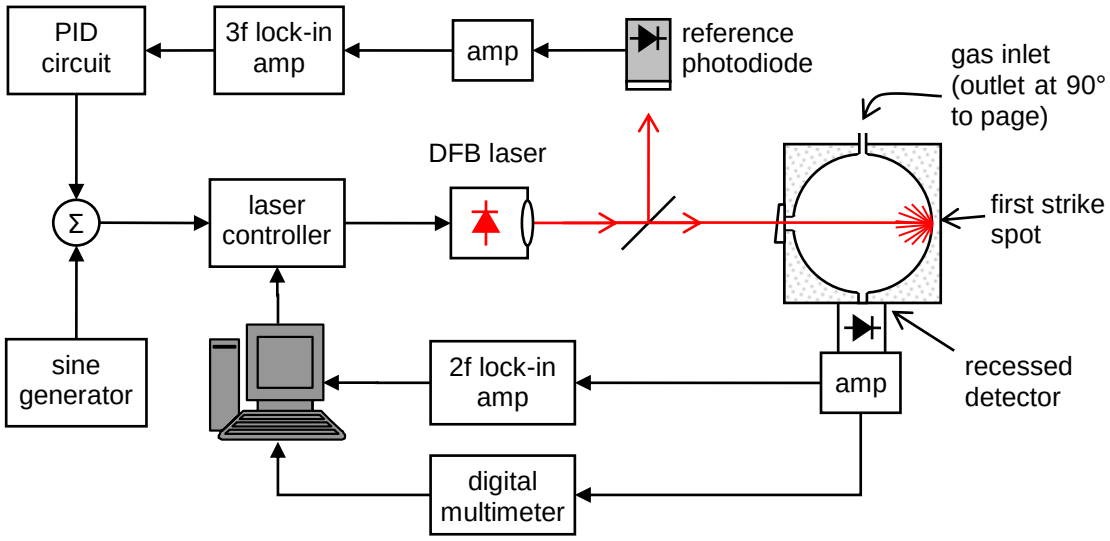

Figure 5. Schematic experimental configuration for 2*f* wavelength modulation spectroscopy, using a 3*f* line lock.

Our integrating sphere (Thorlabs IS200-4, manufactured by Sphere Optics) had an internal diameter of 50.8 mm; for simplicity we term this the "50 mm sphere". Light from the laser diode entered the integrating sphere via a 6.35-mm diameter entry port covered by an angled and antireflection coated window (Thorlabs PS812-C). The detector (12.5 mm diameter port, Thorlabs PDA400) was recessed to prevent a direct line of sight light from the first strike spot, therefore no baffle was necessary. The detector's field of view was restricted to ±32°. Signals from this detector were demodulated using a lock-in amplifier at 2*f* (Stanford SR850). Two additional ports (1.5 mm diameter) allowed entry and exit of test gas mixtures. A digital multimeter (DMM, Keithley 195A) recorded the DC signal.

Test gases were fed to the gas cell from certified cylinders (Scott Specialty Gases), one containing hydrocarbon (HC) free air and the other containing methane in HC free air at a concentration of 2.5%vol. A bank of mass flow controllers (Teledyne Hastings HFC-302 with THPS-400 controller) was used to control flow rates from the two cylinders, with downstream mixing generating different concentrations in the range of 0-2.5 %vol.

5 Results

Experimentally determined 2*f* WMS signals were first normalised using measured DC signals. For the higher concentrations in our range, this could have introduced an error at the line centre caused by the decreased DC transmission. For this reason, we normalised by a DC signal recorded for zero air and assumed that the sphere throughput would be unaltered (eg by misalignment) in subsequent experiments. The calculated and experimentally determined, normalised 2*f* WMS signals are compared in Figure 6.

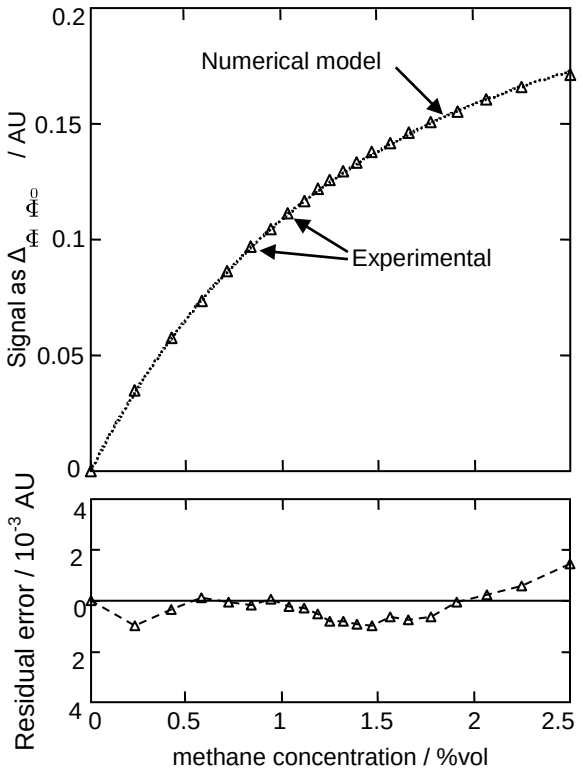

Figure 6. Comparison between predicted and experimentally determined, normalised WMS data. (a) Signal level, (b) residual error.

The low mean residual error of under 10^{-3} AU (as $\Delta I/I_0$) shows that we have good agreement between predicted and experimental results. The fact that the residual error rises consistently for higher concentrations is a result of increased nonlinearity compared to our predictions, which were entirely based on air-broadened lineshapes. This is consistent with the possibility of a change to the underlying absorption profile caused by a gradual change in the gas matrix, which results in increased self-broadening with increasing gas concentration in line with Eq. (4).

In order to compare the level of nonlinearity for normalised WMS signals with that of direct linescans (peak absorbance measurement, previously reported[15]), we rescaled the former by dividing by k = 0.343 (equation (9)) to give identical gradients in the linear regime close to zero gas concentration. The results are shown in Figure 7 and also compared with the results of the Beer-Lambert law, Eq. (1), for a single pass cell with the same equivalent pathlength. This shows, as expected, that the lineshape distortion introduced by our integrating sphere has caused a reduction in both the signal level obtained using direct linescans and, to an even greater extent, the recovered 2*f* WMS signals. The nonlinearity introduced is greater than that expected from the Beer-Lambert law for a single pass cell of equivalent pathlength.

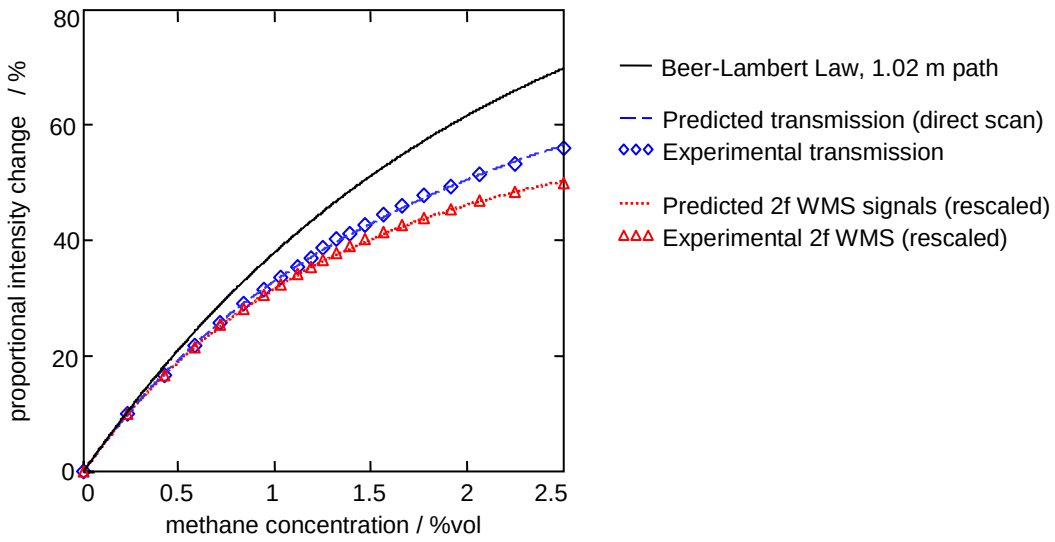

Figure 7. Comparison between predicted and experimental responses for direct transmission and 2*f* WMS measurements, plus the response predicted by the Beer Lambert law for a single pathlength cell. The WMS data has been rescaled, dividing by k=0.343, so as to enable comparison of the relative nonlinearities

We expect the predictions of our model to be sensitive to the value of the modulation index used. In practice, this is often set empirically by maximising the signal obtained from a gas cell. Here, we have assumed that the modulation index is appropriate to a low concentration absorption line with no lineshape distortion. To test the robustness of the model, we performed a sensitivity analysis by altering the modulation index from its optimal value of M=2.2. The results are shown in Table 1 and they indicate that care has to be taken in setting the modulation depth if errors are to be avoided, as the proportional change in WMS signals is an order of magnitude larger than that for conventional, single pass cells (as modelled by Arndt[20]).

Table 1. Results of sensitivity analysis for numerical modelling

Modulation index *m*	Mean residual error for integrating sphere data, as $\Delta\Phi/\Phi_0$	Proportional change in WMS signals	
		Integrating sphere	Single pass cell (calculated from [20])
2.1	5×10^{-3}	14×10^{-3}	1×10^{-3}
2.2	1×10^{-3}	1	1
2.3	3×10^{-3}	8×10^{-3}	1×10^{-3}

6 Discussion and conclusions

Within the linear regime of the Beer-Lambert law, both single pass cells and cells with a distribution of different pathlengths typically provide measurements that are linear functions of the gas concentration in the cell. This applies to measurements made through direct linescans and to recovered 2*f* WMS signals. However, in the nonlinear regime of the Beer-Lambert law, the response in both cases is nonlinear.

We have shown that the nonlinearity obtained using integrating spheres is greater than the conventional nonlinearity expected from the Beer-Lambert law. If the effect were not accounted for, the result might be a 20% error in the estimated gas concentration at a concentration of 2.5 %vol methane. The additional effect arises from a lineshape distortion that exacerbates the problem for 2*f* WMS signals, which experience higher levels of nonlinearity than direct scan measurements. The distortion is introduced by the transfer function of the integrating sphere, which in turn results from the exponential pathlength distribution. Similar effects might therefore also be experienced in cells obeying similar pathlength distributions, such as cavity-enhanced systems.

Our numerical model is supported by experimental data for absorbance in a range of 0-0.17 AU (concentrations of methane in the range of 0-2.5 %vol), for an integrating sphere with internal diameter 5cm. We have not explored the limits of the model here, but could speculate as to where they might lie. Firstly, we can start to see a breakdown of our simplified model as the methane concentrations increases at 2.5% vol. We attribute this to the fact that we did not compensate for increasing levels of self-broadening of the molecular lineshape at higher concentrations. Instead, in order to reduce computation time and complexity in the model, we completed the entire modelling using an air-broadened absorption lineshape, scaling the absorption for different concentrations. This simplification is not fundamental to the modelling of integrating spheres and could be remedied by calculating a different lineshape for each concentration step, using the data in HITRAN[18], though this would be computationally intensive. Secondly, we can ask how accurate our description is of the integrating sphere's transfer function, which relies on an exponential distribution of optical pathlengths. Our previous numerical modelling shows that the pathlength distribution reaches an exponentially decaying asymptote after the light has made a small number of passes (4-6) across the integrating sphere[15]. We might therefore speculate that, should the absorbance within the sphere increase to a level where much of the light was absorbed before making around 6 passes, errors would grow in the model. In this speculation, we should be mindful that even this previous modelling has itself only been experimentally validated for absorbances in the range of 0-0.17 AU.

We calibrated our integrating sphere's equivalent pathlength by measuring the nonlinearity in the peak absorbance of directly scanned gas lines, according to the method outlined in Ref. [15], yielding $Z_{eff} = 1.02 \pm 0.01$ m. In principle, it might also be possible to estimate the value of Z_{eff} by calculating the ringdown time, and to plot directly the distribution of optical pathlengths. Fry *et al*[14] have measured the ringdown decay in intensity, with a ringdown time of $\bar{t} = 30.5$ ns for a 5-cm diameter sphere (made from a new material) with mean wall reflectivity of 99.64%, yielding an equivalent pathlength of 9.15 m. However, there are potential problems with this approach. For our sphere, we would expect a ringdown

time of $\bar{t} \sim 3.4$ ns, and to achieve the same level of measurement precision as with our method (a proportional error of around 1% in Z_{eff}) would require a time measurement resolution at the level of 30 ps. This would place stringent requirements on both the photodetector bandwidth and on the width of the initial laser pulse (Fry *et al* used a pulse width of 11 ns in their work[14]), noting also that the calibration must be performed at the wavelength of the gas absorption line. Secondly and more importantly, many integrating sphere materials are bulk diffuse scatterers, including both the Zenith™ material used in our experiments and the new material of Fry et al.[14]. In these materials, photons penetrate a considerable depth (up to 10mm) into the material and back out, being multiply scattered along this journey. There is therefore an additional (unquantified) pathlength for photons within the sphere material that does not represent the equivalent optical pathlength of the gas cell, the distance over which those photons interact with the gas, giving erroneous results for temporal measurement of the latter. For this reason alone, we consider our approach to calibration to be a more robust method for estimating equivalent pathlengths and the mean internal reflectivities of integrating spheres.

The nonlinearity of an integrating sphere at high gas concentrations can be predicted through numerical modelling. The model is time-consuming, but could for example be represented as a look-up table for a particular gas. However, the predictions of the model are very sensitive to the modulation index, which is often set empirically during experiments. The level of sensitivity is an order of magnitude greater than that experienced in conventional single pass cells. This also means that the degree of nonlinearity will be dependent on pressure fluctuations in the sample; as the pressure changes, so does the linewidth and therefore the modulation index. In the linear regime of the Beer-Lambert law, these changes can be accommodated to give accurate concentration measurements[27l]. However, predicting the integrating sphere nonlinearity in the face of a changing modulation index could be a challenge for real systems, which can often be required to operate over a wide range of gas concentrations, into the nonlinear regime.

Acknowledgements

This work was carried out under an EPSRC research grant (GR/T04601/01) and an EPSRC Advanced Research Fellowship (GR/T04595/01 – J Hodgkinson).

References

[1] J. U. White, J. Opt. Soc. Am. **32**, 285 (1942)

[2] D. R. Herriott, H. Kogelnik, R. Kompfner, Appl. Opt. **3**, 523 (1964)

[3] S. M. Chernin, E. G. Barskaya, Appl. Opt. **30** (1), 51-58 (1991)

[4] R Engeln, G Berden, R Peeters, G Meijer, Rev. Sci. Instrum. 69, 3763-3769 (1998)

[5] A. O'Keefe, D. A. G. Deacon, Rev. Sci. Instrum. 59, 2544-2551 (1988)

[6] E. Hawe, P Chambers, C. Fitzpatrick, E. Lewis, Meas. Sci. Technol. **18**, 3187-3194 (2007).

[7] E. Hawe, C. Fitzpatrick, P. Chambers, G. Dooly, E. Lewis, Sensor. Actuat. A **141**, 414-421 (2008).

[8] C. G. Venkatesh, R. S. Eng, A. W. Mantz, Appl. Opt. **19** (10) 1704-1710 (1980).

[9] R. M. Abdullin, A. V. Lebedev, Sov. J. Opt. Technol. **55** (3) 139-41 (1988).

[10] S. Tranchart, I. H. Bachir, J. - L. Destombes, Appl. Opt. **35** (36), 7070-7074 (1996).

[11] H. I. Schiff, G. I. Mackay, J. Bechara, Chapter 5 in *Air Monitoring by Spectroscopic Techniques*, M W Sigrist, Ed, M Wiley, New York (1994)

[12] D. Masiyano, J. Hodgkinson, R. P. Tatam, Appl. Phys. B **100** (2), 303-312 (2010)

[13] P. Elterman, Appl. Opt. **9** (9), 2140-2142 (1970)

[14] E. S.Fry, J. Musser, G. W. Kattawar, P.-W. Zhai, Appl. Opt. **45** (36), 9053-9065 (2006)

[15] J. Hodgkinson, D. Masiyano, R. P. Tatam, Appl. Opt. **48** (30), 5748-5758 (2010)

[16] M. A. Khan, K. D. Mohan, A. N. Dharamsi, Proc. SPIE 6378, 63780C (2006)

[17] J. D. Ingle, S. R Crouch, *Spectrochemical analysis*, Prentice Hall, New Jersey (1988).

[18] L. S. Rothman *et al*, J. Quant. Spectrosc. Ra. **60**, 711-739 (1998).

[19] P. Kluczynski, J. Gustafsson, Å. M. Lindberg, O. Axner. Spectrochim. Acta B **56** 1277-1354 (2001)

[20] R. Arndt, J. Appl. Phys. 36 (8), 2522-2524 (1965)

[21] L. M. Manojlovíc and A. S. Marinčíc, Meas. Sci. Technol. **22**, 075303 (2011).

[22] E. S. Fry, G. W. Kattawar, B. D. Strycker, P. – W. Zhai, Appl. Opt. **49** (4), 575-577 (2010)

[23] O. Axner, P. Kluczynski, A. M. Lindberg, J. Quant. Spectrosc. Ra **68**, 299-317 (2001)

[24] A. Hangauer, J. Chen, M.-C. Amann, Appl. Phys. B **90**, 249–254 (2008)

[25] L. S. Rothman *et al*, J. Quant. Spectrosc. Ra. **110**, 533-572 (2009)

[26] Parametric Technology Corporation, Mathcad v. 14.0, PTC Inc, Needham, MA, USA (2007)

[27] J. Chen, A. Hangauer, R. Strzoda, M.-C. Amann. Appl Phys B **100**, 417–425 (2010)